Materials Transactions, Vol. 51, No. 9 (2010) pp. 1677 to 1682
©2010 The Japan Institute of Metals
EXPRESS REGULAR ARTICLE

Wetting Transition of Grain Boundaries in Tin–Rich Indium-Based Alloys and Its Influence on Electrical Properties

Chien-Hsuan Yeh[1,*], Li-Shin Chang[1] and Boris Straumal[2]

[1]*Department of Materials Science and Engineering, National Chung Hsing University, 250, Kuo Kuang Road, 40227 Taichung, Taiwan/R.O.C.*
[2]*Institute of Solid State Physics, Russian Academy of Sciences, 142432 Chernogolovka, Moscow district, Russia*

The microstructural evolution of tin–rich indium-based alloys after the grain boundary wetting phase transition in the (liquid + γ) two-phase region of the tin–indium phase diagram and its influence on the electrical conductivity were investigated. Five tin–indium alloys, $Sn_{75}In_{25}$, $Sn_{70}In_{30}$, $Sn_{65}In_{35}$, $Sn_{60}In_{40}$, and $Sn_{55}In_{45}$, were annealed between 393 and 454 K for 24 h. The melted area of the grain boundary triple junctions and grain boundaries increased with increasing the annealing temperature. The microstructures of as-prepared specimens of $Sn_{75}In_{25}$ and $Sn_{70}In_{30}$ alloys had different amounts of completely wetted grain boundaries after annealing. The XRD results show the changes in phases that underwent the eutectic transformation during quenching from various annealing temperatures. The electrical conductivity of annealed tin–indium specimens with various microstructures was measured. It increased with both annealing temperature and tin content.
[doi:10.2320/matertrans.M2010159]

(Received May 6, 2010; Accepted June 18, 2010; Published August 25, 2010)

Keywords: *grain boundary wetting phase transition, electrical conductivity, tin–indium alloy, grain boundaries, microstructure*

1. Introduction

In the electronics industry, solder alloys are widely applied to join chips to conductor substrates. The most commonly used solders in electronic packaging are Sn–Pb alloys. The Sn–Pb alloys have many desirable properties, but the European Union declared in 2006 that imported electric devices must be Pb-free for both environmental and health-related reasons. Subsequently, the research and development of Pb-free alloys has become a very important subject. Numerous Sn-based alloy systems with various alloying elements, such as Ag, Bi, Zn, and Sb, have already been developed to replace the Sn–Pb alloys.[1–3] Indium has also been used as an alloying element in Sn–In component systems to provide suitable properties for soldering.[4–6]

In recent years, electronic devices have been requested to have a high density and more functionality. Heat is generally produced when these electronic devices are used. The increase in temperature can affect the interface microstructure of solder materials. A common phenomenon is the grain boundary wetting phase transition in polycrystalline materials, such as metals and ceramics.[7] The occurrence of the grain boundary wetting transition depends on the GB energy (σ_{GB}) and solid-liquid interface energy (σ_{SL}).[8] When the σ_{GB} is lower than 2 σ_{SL}, the GB is incompletely wetted and the dihedral angle $\theta > 0°$. However, when σ_{GB} is higher than 2 σ_{SL}, the GB is completely wetted by the liquid phase and $\theta = 0°$. When grain boundary wetting transition occurs, the liquid metal forms in the triple junctions among the solid grains and further penetrates into the grain boundaries.[9] The grain boundary wetting phase transition in polycrystalline alloys is closely related to the geometry of the grain boundary. A grain boundary can be defined by five macroscopic parameters, or degrees of freedom (DoF's). The prevalent scheme of GB uses three variables to describe the misorientation of two grains adjacent to the GB and two variables to describe the inclination of the GB.[10] As a result, the spectra of various GBs are associated with different free energies σ_{GB} in polycrystalline materials. Therefore, the maximal wetting temperature $T_{w,max}$ and minimal wetting temperature $T_{w,min}$ can be found for GBs in polycrystals from minimal and maximal energies σ_{GB}, respectively. When the temperature increases from $T_{w,min}$ to $T_{w,max}$, the fraction of completely wetted GBs increases from 0 to 100%.[11] The GB wetting transition can affect the properties of materials, such as the brittleness, plasticity, thermal conductivity and others.[12–14] Some Pb-free solder alloys, Sn–Zn,[15–17] Sn–Al,[18] Al–Sn–Ga,[19] and others, have already been investigated and their grain boundary wetting phase transition temperatures found. However, the influence of the wetting transition of the grain boundaries in Pb-free alloys on electrical conductivity has seldom been discussed.

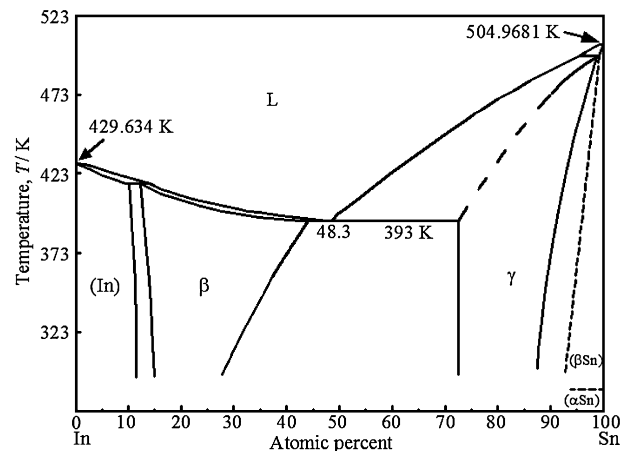

Fig. 1 The Sn–In bulk phase diagram.[20]

Tin–indium alloys have low melting points and the eutectic temperature is 393 K. The Sn–(48–99) at% In alloys with melting points in the range 393–497 K have an extensive (liquid + γ) two-phase region (Fig. 1).[20] Sn–In alloys are also commonly used to replace Pb–Sn solder. They are also

*Graduate Student, National Chung Hsing University

used in cryogenic environments, thermal interface materials, step soldering and heat sensitive-devices among others.[5,21] Since temperature strongly affects Sn–In alloys, the liquid phase is produced in the microstructure. The solidus line of the Sn-rich region in the Sn–In phase diagram has recently been determined.[22] This study aims to observe the microstructural evolution of Sn-rich In alloys that is caused by the grain boundary wetting transition and investigates its effect on electrical conductivity.

2. Experimental

Tin (99.999%) and indium (99.999%) slugs of five compositions were sealed in quartz tubes in an argon atmosphere. The Sn-45, 40, 35, 30, and 25 (at%) In alloys, $Sn_{55}In_{45}$, $Sn_{60}In_{40}$, $Sn_{65}In_{35}$, $Sn_{70}In_{30}$ and $Sn_{75}In_{25}$ respectively, were melted for 10 h at 573 K and homogenized for 24 h at 373 K. These alloy sticks were sliced into several specimens. To obtain uniform microstructures, the specimens were plastically deformed using light blows with a hammer and annealed for 20 h at 383 K.

These Sn-rich In specimens were annealed above the eutectic temperature of 393 K for 24 h to approach the phase equilibrium, and quenched in salt-saturated ice water at 263 K and liquid nitrogen. The deviation of annealing temperatures was controlled within ± 1 K. After they were annealed, the specimens were mechanically ground and then polished using an electro–polishing instrument (Model Tenupol-5, Struers Corporation). The polishing solution contained 70% $HClO_4$ and ethyl alcohol, and the polishing voltage was 30 V. The temperature of the polishing solution was between 233 and 243 K.

The transferred microstructures of annealed specimens were observed using a field-emission scanning electron microscope (FESEM, JSM-6700F, JEOL Instrument). The completely wetted GBs were counted using quantitative metallographic software. Wetted GBs were counted by SEM analysis, using the following criterion: every GB was regarded as completely wetted only when a continuous layer had covered the whole (visible part) of the GB; if such a layer appeared to be interrupted, the GB was regarded as incompletely wetted. Over one hundred GBs were analyzed at each annealing temperature. An X-ray diffractometer (XRD, Model D8 Discover, Bruker Corporation) was used to identify phases of the samples. The XRD parameters were acquired over an angle of diffraction angles, 2θ, between 20° and 80°, with a sampling width of 0.02° and scanning speed of 2°/min. The electrical conductivity of the specimens was measured using the four-probe method. The current source was a Keithley 6221 current source and the voltage was measured using a Keithley 2182A nanovoltmeter. The input currents were 30, 50 and 100 mA. To prevent interference from the environment, the electrical conductivity was measured under vacuum conditions.

3. Results and Discussion

Figure 2 shows the microstructure of $Sn_{75}In_{25}$ specimens annealed for 24 h between 398 and 454 K in the (liquid + γ) two-phase region. A granular structure can be clearly observed in all samples in which the solid grains are γ–$InSn_4$ phase. The grain boundary wetting phase transition is clearly observed. Firstly, the triple junctions and the partial grain boundaries among the solid grains contained the liquid phase during annealing at 398 K. As the annealing temperature increased gradually, more grain boundaries were completely wetted by the liquid phase and the solid grains separated from each other. The liquid phase underwent eutectic transformation and became the β–In_3Sn and irregular γ–$InSn_4$ mixed phase microstructure during quenching. When the annealing temperature approached the liquidus temperature, the liquid phase invaded the grains and occupied most of the area of the specimen. Furthermore, the dendritic γ–phase structure and a small amount of β–phase transformed from the liquid phase during quenching, because the Sn content of the liquid phase increased with annealing temperature close to the liquidus temperature. Figures 2(b) and (c) show small inclusions inside a few grain boundaries after the $Sn_{75}In_{25}$ specimens were annealed at 398 and 404 K. A few of the thinner wetted liquid layers perhaps shrunk and formed the strip of interrupted inclusions in the grain boundaries because of rapid quenching.

Figure 3 shows the microstructures of the $Sn_{70}In_{30}$ specimens after annealing. It reveals that numerous grain boundaries were completely wetted by the liquid phase during annealing for 24 h at 394 K, just 1 K above the eutectic temperature. The liquid layers occupied most of the grain boundaries and their thickness increased gradually with temperature. The extent of grain boundary wetting in $Sn_{70}In_{30}$ specimens was higher than that in $Sn_{75}In_{25}$ specimen at a given annealing temperature (398 K). The microstructure of as-prepared $Sn_{70}In_{30}$ specimens was inferred to be a pearlite-like structure with a high β–phase content (Fig. 3(a)). As the temperature increased over the eutectic temperature, the β–phase and the grain boundaries with higher energy transformed firstly into the liquid phase. Therefore, the phenomenon of completely wetted GBs in $Sn_{70}In_{30}$ specimens can be clearly observed after annealing at 398 K. Figure 4 shows the annealed microstructures of other Sn–rich In alloys, $Sn_{65}In_{35}$, $Sn_{60}In_{40}$ and $Sn_{55}In_{45}$ alloys. Almost all of the grain boundaries in these Sn–In alloys were occupied by the liquid phase layers. As the Sn content decreased close to the eutectic composition, the number of solid grains decreased gradually and the liquid phase became the major phase in the structure.

Figure 5 shows the statistical results for the completely wetted GBs of Sn-rich In alloys at various annealing temperatures. The fraction of GBs that are completely wetted depends on the annealing temperature. When the $Sn_{75}In_{25}$ alloy was annealed between 398 and 437 K, the fraction of completely covered GBs increased from 13 to 84% with the annealing temperature. Upon annealing at 437 K, the number of solid grains decreased gradually and the liquid layer transformed into a large liquid phase region among the grains, making the fraction of completely wetted GBs difficult to determine correctly. The fraction of completely wetted GB in the annealed $Sn_{70}In_{30}$ alloy also depends on the annealing temperature. Between 394 and 424 K, the fraction of wetted GBs gradually increased from 78 to 91% with temperature. The proportion, 78%, of the GBs that were

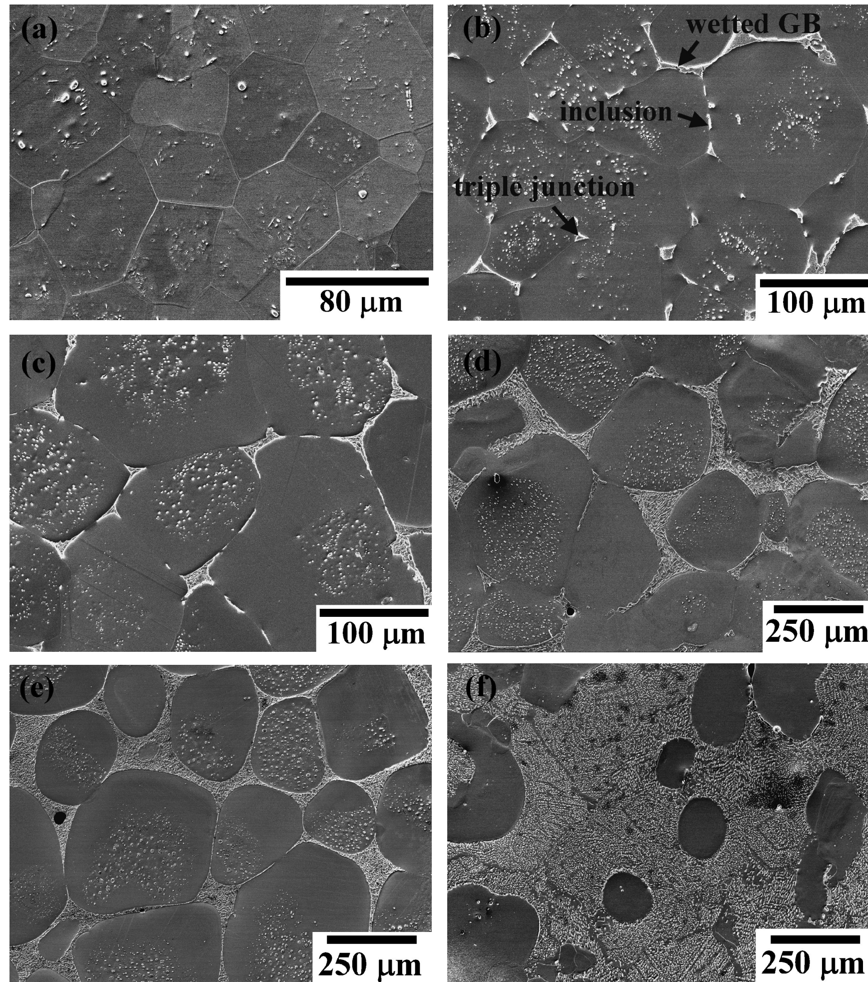

Fig. 2 Micrographs of (a) the as-prepared $Sn_{75}In_{25}$ specimens and annealed for 24 h at (b) 398, (c) 404, (d) 414, (e) 424 and (f) 454 K.

completely wetted by annealing at 394 K, which is slightly above the eutectic temperature is such that the minimal wetting temperature $T_{w,min}$ can not be found within the (liquid + γ) two phases region of the Sn–In phase diagram. Figure 5 plots statistical results concerning wetted GBs in other Sn-rich In alloys that were annealed for 24 h at 398 K. The fractions of completely wetted GBs of these alloys were between 92 and 96%. Only a few grain boundaries with lower energy were not wetted by the liquid phase in the annealed alloys. The amount of completely wetted GBs (at a given annealing temperature) increased with indium content in the alloys (Fig. 5), because the amount of liquid phase in the microstructure increased during annealing.

The grain boundary wetting phase transition alters the microstructure of Sn-rich In alloys and also affects their crystal structures during quenching. Figure 6 shows the XRD results of the $Sn_{75}In_{25}$ alloy via annealing at 398 to 445 K. These results reveal that directly after homogenization, the initial $Sn_{75}In_{25}$ alloy was composed of the non-stoichiometric γ phase. A liquid phase formed in the γ-matrix during annealing in the solid-liquid phase region, as revealed by the XRD patterns, which indicate that the annealed $Sn_{75}In_{25}$ samples contained a small amount of β–phase. Figure 7 shows the XRD pattern of five Sn-In alloys after annealing for 24 h at 398 K. The peak height of the β–phase clearly increases as the Sn content decreases since the quantity of liquid phase increased during the isothermal annealing and more β–phase was formed during quenching.

Since grain boundary wetting can cause microstructural variations and affects the properties of polycrystalline materials, the electrical properties of the annealed Sn-rich In solder alloys was investigated in the present study. Figure 8(a) plots variations in electrical conductivity of the $Sn_{75}In_{25}$ alloy. The electrical conductivity of the as-prepared $Sn_{75}In_{25}$ specimen, which had a clear granular structure and completely dry grain boundaries, is about 50,225 $(\mathrm{Ohm{\cdot}cm})^{-1}$. When the $Sn_{75}In_{25}$ specimens were annealed above the eutectic temperature, the liquid phase wetted the triple junctions and grain boundaries. With increasing annealing temperature, the Sn content of the γ–phase solid grains and the liquid phase both increased. The fraction of β–phase decreased gradually during quenching. The γ–phase structure became the dendritic structure from irregular structure with the amount of γ–phase. A dendritic structure grew from the liquid phase and then extended to connect adjacent solid grains during quenching from the higher annealing temperature (Fig. 9(a)–(c)). The connected dendritic γ–phase structure can be regarded as electronic conductive channels. After annealing, as GB wetting proceeds, the electrical conductivity of the $Sn_{75}In_{25}$ alloy increased gradually with annealing temperature and the fraction of γ–phase. Figure 8(b) plots the electrical con-

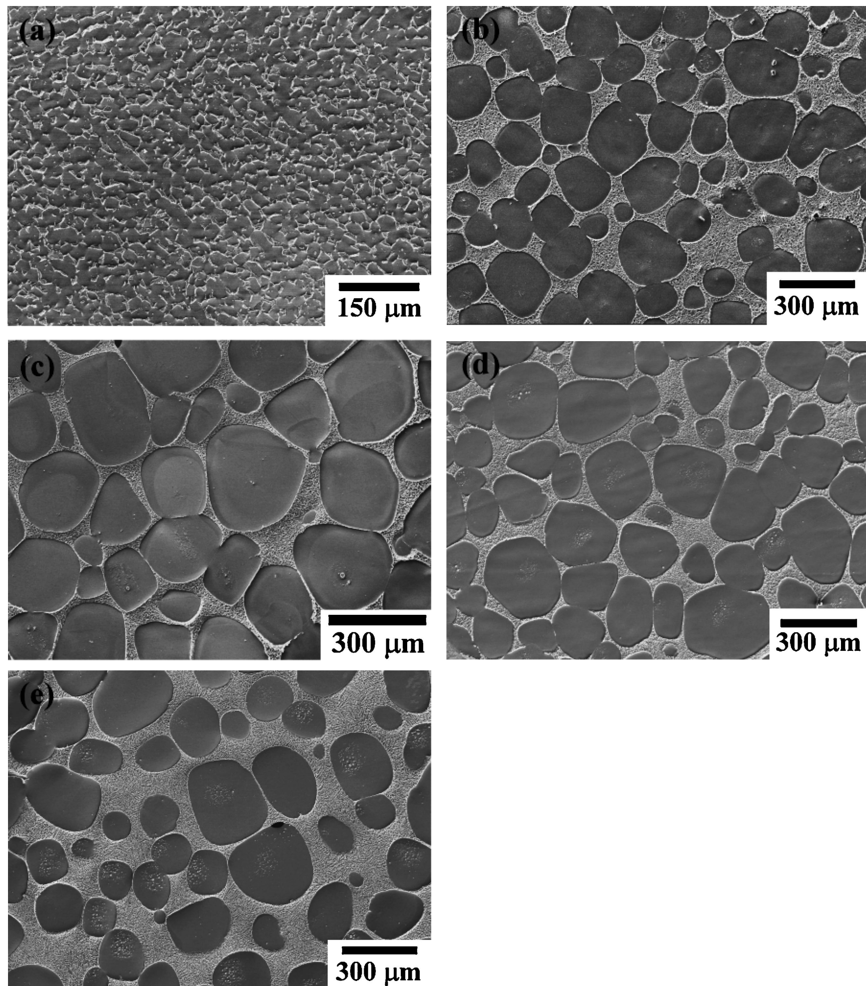

Fig. 3 Micrographs of (a) the as-prepared $Sn_{70}In_{30}$ specimens and annealed for 24 h at (b) 394, (c) 398, (d) 404, and (e) 424 K.

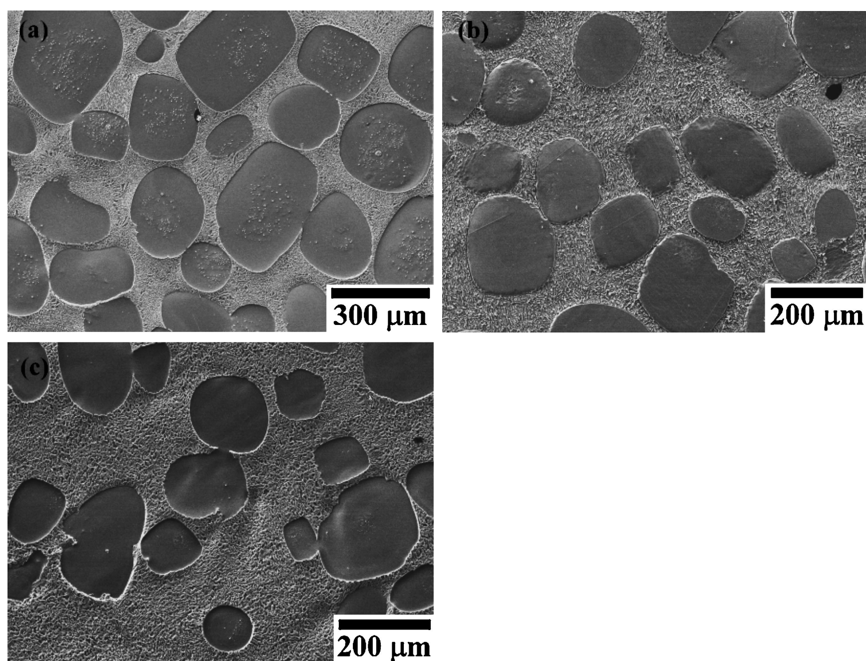

Fig. 4 Micrographs of (a) $Sn_{65}In_{35}$, (b) $Sn_{60}In_{40}$ and (c) $Sn_{55}In_{45}$ alloys after annealing for 24 h at 398 K.

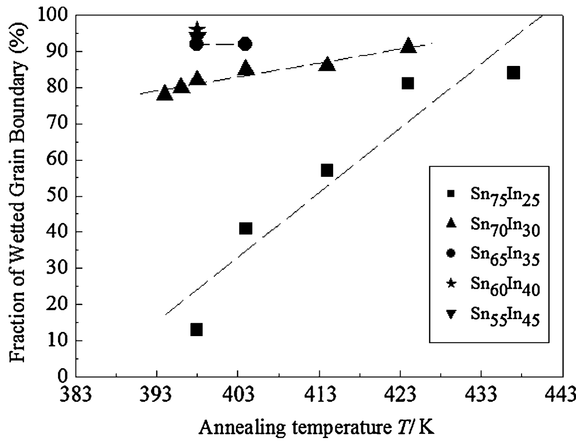

Fig. 5 Fraction of the completely wetted GBs related to the annealing temperature for Sn-rich In alloys.

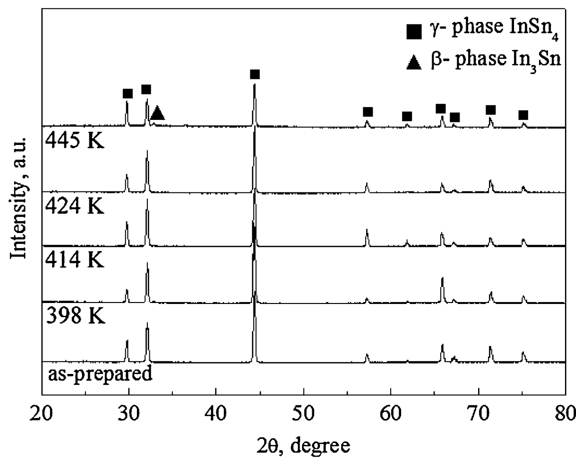

Fig. 6 XRD pattern of the $Sn_{75}In_{25}$ alloy annealed at 398 to 445 K.

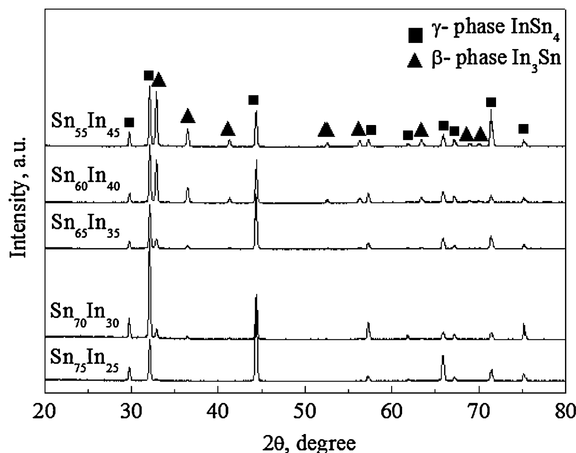

Fig. 7 XRD pattern of the $Sn_{75}In_{25}$, $Sn_{70}In_{30}$, $Sn_{65}In_{35}$, $Sn_{60}In_{40}$ and $Sn_{55}In_{45}$ alloys annealed for 24 h at 398 K.

ductivity of five Sn-rich In alloys annealed at 398 K. The electrical conductivity of the annealed $Sn_{75}In_{25}$ specimen is about 51,481 $(\mathrm{Ohm{\cdot}cm})^{-1}$. When these Sn-rich In alloys annealed at 398 K, the amount of liquid phase increased and the number of solid grains decreased with the In content. The composition of liquid phase contained lower Sn content. According to the XRD results, the amount of β–phase

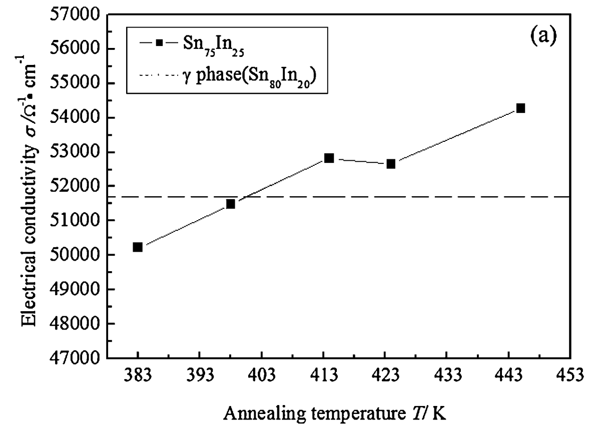

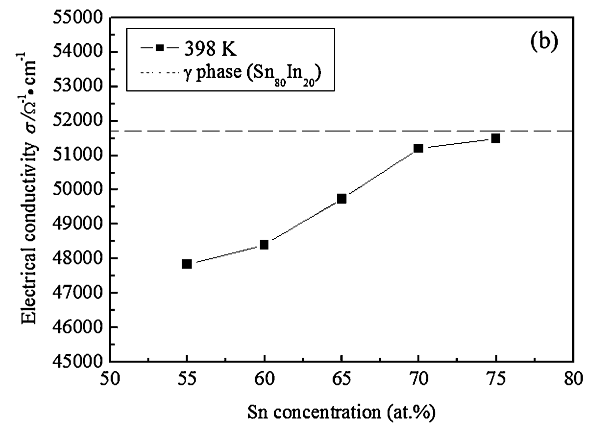

Fig. 8 The electrical conductivity of (a) $Sn_{75}In_{25}$ specimens annealed at various temperatures and (b) five Sn-In alloys annealed at 398 K (The dash line indicates the electrical conductivity of the γ-phase ($Sn_{80}In_{20}$ alloy)).

increases as the amount of liquid phase increases. The β–phase surrounded the fine and irregular γ phase grains (Fig. 9(d)). This variation reduces electrical conductance.

4. Conclusions

Five Sn-rich In alloys, $Sn_{75}In_{25}$, $Sn_{70}In_{30}$, $Sn_{65}In_{35}$, $Sn_{60}In_{40}$ and $Sn_{55}In_{45}$, were annealed in the (liquid + γ) two-phase region to investigate their microstructural evolution after the grain boundary wetting phase transition, and its effect on electrical conductivity. In $Sn_{75}In_{25}$ alloy, the fraction of wetted GBs gradually increases from 13 to 84% as the temperature increases from 398 and 437 K. In $Sn_{70}In_{30}$ alloy, the fraction of wetted GBs gradually increases from 78 to 91% as temperature increases from 394 to 424 K. The amount of the completely wetted GBs increased (at a given annealing temperature) as the indium content in the alloys increased, because the relative among of liquid phase in the microstructure increased during annealing. During quenching, the liquid phase layer transferred into the β–In_3Sn phase and γ–$InSn_4$ phase structures, depending on the amount and composition of the liquid phase. The electrical conductivity of the $Sn_{75}In_{25}$ alloy increases with annealing temperature because the connected dendritic γ–phase structure forms and the Sn content increases. Annealing Sn-rich In alloy at 398 K reduces its electrical conductivity because it increases the amount of β–phase structure.

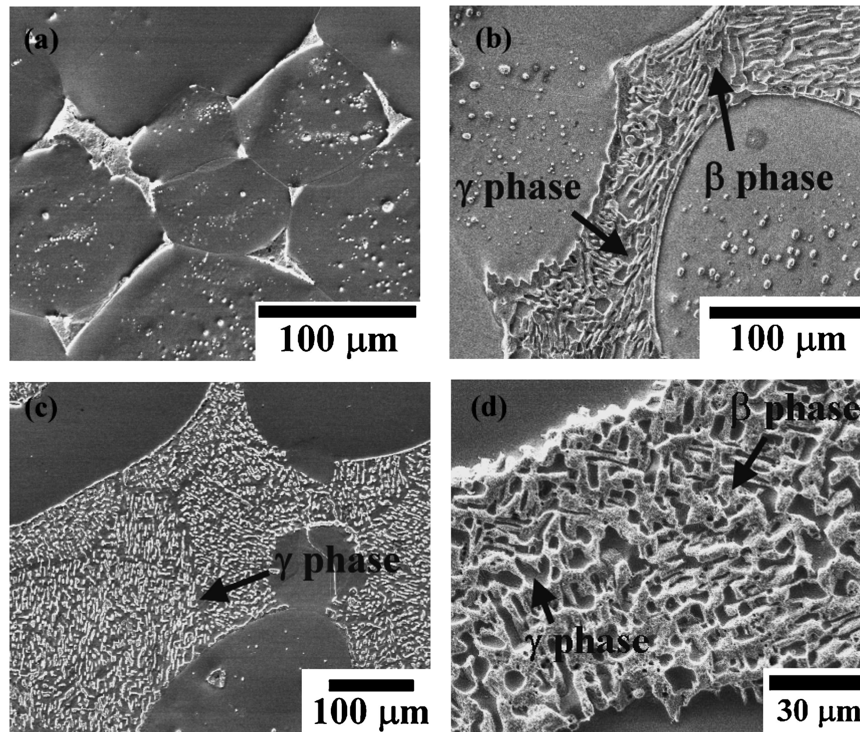

Fig. 9 Micrographs of the $Sn_{75}In_{25}$ specimens annealed at (a) 398, (b) 414, (c) 445 K and (d) the $Sn_{55}In_{45}$ specimen annealed at 398 K. The liquid phase transforms into the γ-phase and β-phase after quenching.

Acknowledgements

This work was financially supported by the Russian Foundation for Basic Research under the contract 05-03-90578 and National Scientific Council of Taiwan under the contracts NSC 96-2218-E-005-015.

REFERENCES

1) S. K. Kang and A. K. Sarkhel: J. Electron. Mater. **23** (1994) 701–707.
2) Q. L. Yang and J. K. Shang: J. Electron. Mater. **34** (2005) 1363–1367.
3) S. W. Chen, C. H. Wang, S. K. Lin and C. N. Chiu: J. Mater. Sci. Mater. Electron. **18** (2006) 19–37.
4) R. M. Shalaby and M. El-Sayed: Radiat. Eff. Defects Solids **160** (2005) 23–31.
5) D. G. Kim and S. B. Jung: J. Alloy. Compd. **386** (2005) 151–156.
6) W. K. Jones, Y. Liu, M. Shah and R. Clarke: Solder. Surf. Mt. Technol. **10** (1998) 37–41.
7) D. R. Clarke: Mater. Sci. Forum **294–296** (1996) 1–8.
8) B. B. Straumal, P. Zieba and W. Gust: Int. J. Inorg. Mater. **3** (2001) 1113–1115.
9) B. B. Straumal, O. Kogtenkova and P. Zieba: Acta Mater. **56** (2008) 925–933.
10) M. Takashima, P. Wynblatt and B. L. Adams: Interface Sci. **8** (2000) 351–361.
11) B. Straumal and B. Baretzky: Interface Sci. **12** (2004) 147–155.
12) W. Ludwig, E. Pereiro-López and D. Bellet: Acta Mater. **53** (2005) 151–162.
13) B. Straumal, N. E. Sluchanko and W. Gust: Defect Diff. Forum **188–190** (2001) 185–194.
14) G. Pezzotti, A. Nakahira and M. Tajika: J. Eur. Ceram. Soc. **20** (2000) 1319–1325.
15) B. B. Straumal, W. Gust and T. Watanabe: Mater. Sci. Forum **294–296** (1999) 411–414.
16) V. Murashov, B. Straumal and P. Protsenko: Defect Diff. Forum **249** (2006) 235–238.
17) A. S. Gornakova, B. B. Straumal, S. Tsurekawa, L.-S. Chang and A. N. Nekrasov: Rev. Adv. Mater. Sci. **21** (2009) 18–26.
18) B. Straumal, W. Gust and D. Molodov: J. Phase Equilib. **15** (1994) 386–391.
19) B. Straumal, S. Risser, V. Sursaeva, B. Chenal and W. Gust: J. Phys. IV **5** (1995) 233–241.
20) T. B. Massalski, H. Okamoto, P. R. Subramanian and L. Kacprzak: *Binary Alloy Phase Diagrams*, (ASM International, Materials Park, OH, 1990) pp. 2295–2296.
21) I. Dutta, R. Raj, D. Suh and V. Wakharkar: 9th Electronics Packaging Technology Conference, (Singapore, 2007) pp. 365–369.
22) C.-H. Yeh, L.-S. Chang and B. Straumal: J. Phase Equilib. Diffus. **30** (2009) 254–257.